THE JOURNAL OF BIOLOGICAL CHEMISTRY
Vol. 279, No. 22, Issue of May 28, pp. 23349–23356, 2004
Printed in U.S.A.
© 2004 by The American Society for Biochemistry and Molecular Biology, Inc.

Binding Stoichiometry and Kinetics of the Interaction of a Human Anthrax Toxin Receptor, CMG2, with Protective Antigen*

Received for publication, February 5, 2004, and in revised form, March 22, 2004
Published, JBC Papers in Press, March 24, 2004, DOI 10.1074/jbc.M401292200

Darran J. Wigelsworth‡, Bryan A. Krantz‡, Kenneth A. Christensen, D. Borden Lacy, Stephen J. Juris, and R. John Collier§

From the Department of Microbiology and Molecular Genetics, Harvard Medical School, Boston, Massachusetts 02115

The protective antigen (PA) moiety of anthrax toxin binds to cellular receptors and mediates entry of the two enzymatic moieties of the toxin into the cytosol. Two PA receptors, anthrax toxin receptor (ATR)/tumor endothelial marker 8 (TEM8) and capillary morphogenesis protein 2 (CMG2), have been identified. We expressed and purified the von Willebrand A (VWA) domain of CMG2 and examined its interactions with monomeric and heptameric forms of PA. Monomeric PA bound a stoichiometric equivalent of CMG2, whereas the heptameric prepore form bound 7 eq. The K_d of the VWA domain-PA interaction is 170 pM when liganded by Mg^{2+}, reflecting a 1000-fold tighter interaction than most VWA domains with their endogenous ligands. The dissociation rate constant is extremely slow, indicating a 30-h lifetime for the CMG2·PA monomer complex. CMG2 metal ion-dependent adhesion site (MIDAS) was studied kinetically and thermodynamically. The association rate constant ($\sim 10^5$ M^{-1} s^{-1}) is virtually identical in the presence or absence of Mg^{2+} or Ca^{2+}, but the dissociation rate of metal ion liganded complex is up to 4 orders of magnitude slower than metal ion free complex. Residual affinity ($K_d \sim 960$ nM) in the absence of divalent metal ions allowed the free energy for the contribution of the metal ion to be calculated as 5 kcal mol^{-1}, demonstrating that the metal ion-dependent adhesion site is directly coordinated by CMG2 and PA in the binding interface. The high affinity of the VWA domain for PA supports its potency in neutralizing anthrax toxin, demonstrating its potential utility as a novel therapeutic for anthrax.

The pathology of the anthrax bacillus, *Bacillus anthracis,* is due in part to the production of anthrax toxin, an ensemble of three nontoxic monomeric proteins that combine at the surface of host cells to form toxic noncovalent complexes (see Fig. 1*A*). Two of these proteins are enzymes that modify cytosolic substrates. Lethal factor (LF,[1] 90 kDa) is a Zn^{2+} protease that cleaves several mitogen-activated protein kinase kinases (1, 2), and edema factor (EF, 89 kDa) is a Ca^{2+}- and calmodulin-dependent adenylate cyclase (3). The third protein, protective antigen (PA_{83}, 83 kDa), binds to cellular receptors and transports LF and EF to the cytosol.

The initial step in the action of the toxin is the binding of PA to a cell surface receptor. Receptor-bound PA is cleaved into two fragments by a furin family protease (4). Dissociation of the smaller fragment allows the larger fragment, which remains receptor-bound, to self-associate into ring-shaped heptamers ($(PA_{63})_7$, also referred to as prepore (5)). Prepore may then bind up to three molecules of LF and/or EF with nanomolar affinity (6, 7). The resulting complexes are endocytosed to an acidic compartment (8, 9), where the heptamers are converted from the prepore state to an integral membrane, ion-conductive pore (10). The process of translocating LF and EF into the cytosol is linked to the formation of pore, but the nature of this linkage is poorly understood. Within the cytosol these enzymatically active moieties may then disrupt normal cellular physiology.

Two anthrax toxin receptors, CMG2 (11) and anthrax toxin receptor (ATR)/tumor endothelial marker 8 (12), are known. Each is a single peptide chain consisting of an extracellular domain, a membrane-spanning region, and a cytoplasmic tail. In their extracellular domains, there is an ~200-amino acid von Willebrand type A (VWA) domain that shows 60% amino acid identity between the two proteins (11). This domain adopts a dinucleotide binding or Rossmann fold that is composed of a sandwich of six eight amphipathic α-helices that surround a hydrophobic β-sheet (see Fig. 1*B*).[2] The VWA domain fold is found in many cell adhesion proteins and generally promotes protein-protein interactions (13). Many VWA domains contain a highly conserved metal ion-dependent adhesion site (MIDAS) that is often involved in ligand interactions (14). The metal ion adopts an octahedral geometry and is coordinated by residues from three of its loops as well as two to three ordered water molecules. Usually, a glutamic or aspartic acid side chain from the ligand completes this metal ion coordination sphere; therefore, the metal ion acts as a bridge between the ligand and VWA domain. Consistent with a metal ion-mediated interaction, both CMG2 and ATR have been shown to bind PA more tightly in the presence of divalent cations (11, 12).

Here, we quantify the binding interaction of soluble CMG2 VWA domain with PA_{83} monomer and PA_{63} heptamer. Mono-

* The costs of publication of this article were defrayed in part by the payment of page charges. This article must therefore be hereby marked "*advertisement*" in accordance with 18 U.S.C. Section 1734 solely to indicate this fact.

‡ These authors contributed equally to this work.

§ To whom correspondence should be addressed. Dept. of Microbiology and Molecular Genetics, Harvard Medical School, 200 Longwood Ave., Boston, MA 02115. Tel.: 617-432-1930; Fax: 617-432-0115; E-mail: john_collier@hms.harvard.edu.

[1] The abbreviations used are: LF, lethal factor; LF_N, LF amino-terminal domain (residues 1–263); EF, edema factor; AF488, Alexa Fluor 488; AF546, Alexa Fluor 546; CMG2, capillary morphogenesis protein 2; $CMG2^{35–225}$, VWA domain of CMG2 residues 35–225; $CMG2^{C40}$, $CMG2^{R40}$ with point mutations R40C and C175A; $CMG2^{R40}$, CMG2 residues 40–217; NEM, *N*-ethylmaleimide; $CMG2^{C40}$-NEM, $CMG2^{C40}$ modified by NEM; FRET, fluorescence resonance energy transfer; MIDAS, metal ion-dependent adhesion site; PA_{83}, monomeric protective antigen precursor; PA_{20}, amino-terminal domain of PA_{83}; PA_{63}, individual monomer in the heptameric form of protective antigen; $(PA_{63})_7$, heptameric protective antigen; VWA domain, von Willebrand A domain; $\Delta\Delta G^{M2+}$, binding free energy change due to the presence of a divalent cation; MES, 2-(*N*-morpholino)ethanesulfonic acid; ATR, anthrax toxin receptor; GST, glutathione *S*-transferase; SPR, surface plasmon resonance; PA, protective antigen; NIF, neutrophil inhibitory factor.

[2] D. B. Lacy, D. J. Wigelsworth, H. M. Scobie, J. A. T. Young, and R. J. Collier, submitted for publication.

Downloaded from www.jbc.org by on July 7, 2008

meric PA bound a stoichiometric equivalent of CMG2, whereas the heptameric prepore form bound 7 eq. The equilibrium dissociation constant (K_d) for CMG2 VWA domain interaction with monomeric PA_{83} is very tight (170 pM), and the dissociation rate constant is extremely slow ($\sim 10^{-5}$ s^{-1}). We show that the tight binding affinity relies on the presence and identity of the divalent MIDAS metal ion. Knowledge of the affinity and slow dissociation rate of CMG2·PA complexes supports the notion that CMG2 VWA domain may be used clinically as an inhibitor of anthrax toxin.

MATERIALS AND METHODS

Plasmid Construction—A DNA sequence encoding residues 35–225 of the CMG2 VWA domain (referred to as $CMG2^{35-225}$) was cloned into pGEX4T-1 (Amersham Biosciences) using 5′ BamHI and 3′ NotI restriction sites. pGEX4T-1 includes a thrombin-cleavable glutathione *S*-transferase tag onto the amino terminus of the expressed protein. Two truncated versions of CMG2 were then generated using PCR and the same 5′ BamHI and 3′ NotI sites, (i) residues 38–218 ($CMG2^{S38}$) and (ii) residues 40–217 ($CMG2^{R40}$). The latter version eliminated the natural disulfide bond. To generate a version of CMG2 with a single, unique cysteine point mutation on the amino terminus, two successive rounds of site-directed mutagenesis were performed on $CMG2^{R40}$. The C175A mutation was introduced to eliminate the remaining buried cysteine, and the R40C mutation created a unique cysteine residue on the more accessible amino terminus, making $CMG2^{C40}$.

Preparation of Proteins—Recombinant lethal factor amino-terminal domain (residues 1–263; LF_N) was purified as described previously (15). Recombinant PA was expressed in BL21(DE3) using pET22b-PA (Novagen), which directs expression to the periplasm. Growth and expression of PA was carried out in a 10-liter Bioflo 110 fermenter (New Brunswick Scientific). Using ECPM1 growth media (16), cells were grown at 37 °C to ~5 $A_{600\ nm}$ units, sparged by a 60% air, O_2 mixture, and induced at 30 °C using 1 mM isopropyl-1-thio-β-D-galactopyranoside. PA was extracted from the periplasm and further purified using Q-Sepharose anion-exchange chromatography (Amersham Biosciences) in 20 mM Tris, pH 8.0 (Buffer A), and Buffer A + 1 M NaCl (Buffer B). The protein was further purified using an S-200 Superdex gel filtration column (Amersham Biosciences) in Buffer A. For fluorescence studies PA_{83} with either the K563C or E733C point mutation was purified as described previously (15) and stored at −80 °C in 10 mg/ml aliquots in 10 mM dithiothreitol.

CMG2 VWA domain variants were grown in a similar way, except induction was carried out at 37 °C. Harvested bacteria were lysed by French press and sonication. GST-CMG2 was loaded onto a ~50-ml glutathione-Sepharose 4B column (Amersham Biosciences), the column was washed in Buffer A, and bound fusion was cleaved from the immobilized GST using bovine α-thrombin (Sigma) overnight at room temperature. Thrombin was removed from the eluate with benzamidine-Sepharose, and CMG2 was further purified using an S-200 Superdex column (Amersham Biosciences). The purified stock protein solution was concentrated to 10 mg/ml, 10 mM dithiothreitol was added to protect the free thiol, and the solution was frozen at −80 °C.

Fluorescence Labeling and Modification of PA and CMG2—Buffers A and B were purged by sparging with N_2 for 5 min, and 0.5 mM tris-(2-carboxyethyl)phosphine was added to each buffer. An S-200 gel filtration column was preequilibrated with 15% Buffer B. Approximately 20 mg of either PA_{83} K563C, PA_{83} E733C, or $CMG2^{C40}$ was purified using gel filtration to remove excess dithiothreitol, which would react with the maleimide-activated fluorophores. One mg of either maleimide thiol reactive fluorophore, Alexa Fluor 488 (AF488) or Alexa Fluor 546 (AF546), was added to each protein eluate in approximately a 10-ml volume (2 mg/ml final protein concentration) for 2 h at room temperature. Two separate preparations of PA_{83} K563C were labeled with AF488 donor and AF546 acceptor; PA_{83} E733C was labeled with the donor AF488, making PA_{83} E733C-AF488, and $CMG2^{C40}$ was labeled with the acceptor AF546, making $CMG2^{C40}$-AF546. After the completion of the reaction, unreacted dye reagent was blocked with 10 mM 2-mercaptoethanol, and labeled protein was subsequently purified from free dye by a second round of S-200 gel filtration using 15% Buffer B in the absence of tris-(2-carboxyethyl)phosphine. Protein solutions were assessed for labeling efficiency using predetermined extinction coefficients for the fluorophores at their respective absorbance maxima and 280 nm. Labeling efficiency was 95% or greater. Uniformly labeled PA heptamer, $(PA_{63})_7$ E733C-AF488, was generated as previously described (17). Using an identical procedure, $CMG2^{C40}$ was blocked at the reactive cysteine by *N*-ethylmaleimide (NEM), creating $CMG2^{C40}$-NEM.

Isothermal Titration Calorimetry—Experiments were carried out using a VP-ITC calorimeter (Microcal) at 30 °C. PA_{83} monomer (5 μM) and $CMG2^{35-225}$ (70 μM) were degassed at 30 °C under vacuum. Multiple injections of $CMG2^{35-225}$ were made into the PA_{83}-containing measurement cell under continuous stirring. Data were analyzed using Microcal Origin software.

Fluorescence Equilibrium Stoichiometry Titration—PA_{83} E733C-AF488 was diluted to 1 μM in 2 ml of universal buffer, 10 mM each Tris, MES, HEPES, and acetic acid, and 0.1 mg/ml bovine serum albumin, pH 8.0, that was supplemented with 1 mM $MgCl_2$. 100-μl aliquots were iteratively removed after the addition of sub-stoichiometric quantities of $CMG2^{C40}$-AF546, thereby continually increasing the molar ratio of $CMG2{\cdot}PA_{83}$ during the titration from 0.1 to 5.2. Each 100-μl aliquot was separately incubated for about 1–2 h at room temperature to ensure complete binding.

Similarly, $(PA_{63})_7$ E733C-AF488 was diluted to 16 nM; however, 0.5 μM LF_N was added to the reaction mixture to minimize nonspecific interactions with the PA-LF binding face. The molar ratio was varied as described for PA_{83} except the range spanned 0.3–25.

Each aliquot was then analyzed in an ISS fluorimeter interfaced to an Ar^+ laser. The 488-nm line was used for excitation of the donor fluorophore (AF488). Donor and acceptor emission were acquired at 520 and 570 (±10) nm, respectively. The apparent fluorescence resonance energy transfer (FRET) signal was defined by the ratio of the acceptor to donor fluorescence emission. Aliquots were diluted to 2 ml in universal buffer. Fluorescence counts were recorded for 10 s, and all aliquots in a given titration were measured in triplicate.

Multiangle Laser Light Scattering—Approximately 200–400 μg of protein was loaded in specific mixtures onto a Shodex KW-803 column at a flow rate of 0.5 ml min^{-1} in 20 mM Tris-Cl, 200 mM NaCl, pH 8.5. The column was connected to a DAWN EOS 18-angle light scattering detector and an OPTILAB DSP interferometric refractometer (Wyatt Technology). Detectors 6–15 were used. A refractive index increment value (*dn/dc*) of 0.185 ml/g was used. Detectors were normalized to compensate for slight differences in electronic gain using bovine serum albumin as an isotropic scatterer. Data were analyzed using ASTRA software.

Kinetics of PA_{63} Heptamerization—The FRET-based kinetics assay was used to monitor the rate of heptamerization for PA_{63}. A reaction mixture of fluorescently labeled nicked PA_{83} (50 nM each donor, AF488, and acceptor, AF546) in 20 mM Tris-Cl, 150 mM NaCl, 1 mM Ca^{2+}, 0.1 mg/ml bovine serum albumin, pH 8.5, was either preincubated with no $CMG2^{35-225}$ or 1 μM $CMG2^{35-225}$ at 20 °C for 15 min. At time 0 each heptamerization reaction was initiated by the addition of 100 nM LF_N. Control experiments were performed in the absence of LF_N. Kinetic profiles were recorded using the ISS fluorimeter (excitation, 488 nm), where the emission at 520 and 570 (±10) nm reflected the increase in apparent FRET upon heptamerization. Time points were taken automatically every 15 s for 7×10^3 s.

Surface Plasmon Resonance Analysis—All experiments were performed using the Biacore 2000 system sensor chips. For CM5 chips, the system was maintained at a constant flow rate of 5 μl min^{-1} of HBS buffer (10 mM HEPES, pH 7.4, 150 mM NaCl) at 25 °C. Monomeric PA_{83} was covalently linked to the carboxylated dextran matrix. Monomeric PA_{83} was diluted to 2 μM in sodium acetate buffer, pH 4.5. The protein was injected onto the activated surface at a flow rate of 5 μl min^{-1} until the desired base-line level of 2000–4000 response units was obtained (~5 min) and then blocked with ethanolamine.

CMG2 VWA domain variants were diluted into HBS running buffer with either 1 mM $CaCl_2$ or 1 mM $CaCl_2$ plus 0.5 mM tris-(2-carboxyethyl)phosphine, pH 7.4, and serial injections were made at 10 μl min^{-1}. Concentrations of protein ranged from 47 nM to 4.8 μM. CM5 base lines were regenerated with a 30-μl pulse of 0.5 M $NaCO_3$, pH 10.5, resulting in <1% loss of base line per injection.

Binding Kinetics Using FRET—All kinetics experiments were conducted at 20 °C. Rates of association between CMG2 and PA were assessed using stopped-flow FRET. A Biologic SFM-400 stopped-flow was fitted to a custom two channel filter fluorimeter. An Ar^+ laser was used for excitation at 488 nm via a fiber optic cable. Two H5784-20 photosensor modules (Hamamatsu) were controlled via the manufacturer's recommended resistance programming circuit; the photosensors collected a fluorescent emission signal after optical filtering (Omega) by a notch, bandpass filter (520–540 nm) in channel 1 and a longpass filter (>560 nm) in channel 2. These emission signals were then electronically filtered by an 11-pole elliptical function filter (TTE, Inc.) before collection by the computer A/D card. During acquisition, the computer

Downloaded from www.jbc.org by on July 7, 2008

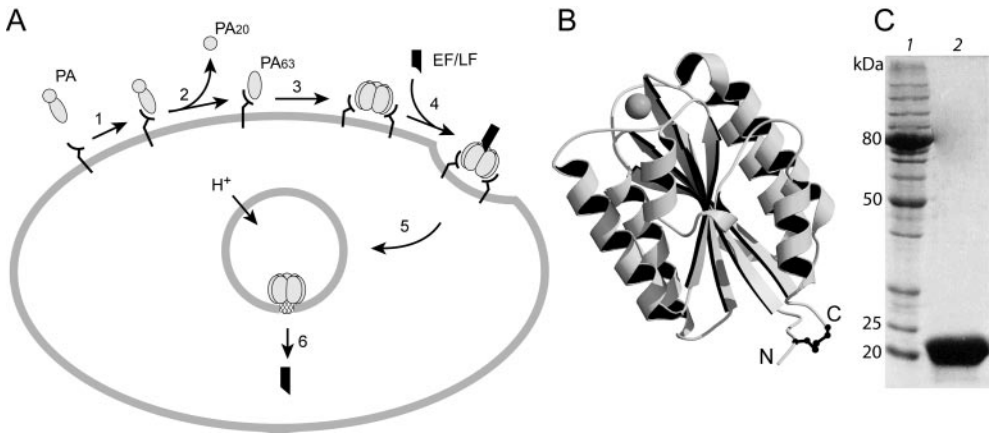

FIG. 1. *A*, model of anthrax toxin entry into cells emphasizes the important role of the receptor in toxin complex assembly and internalization: *1*, binding of PA_{83} to its receptor (CMG2 or ATR/ tumor endothelial marker 8); *2*, proteolytic activation of PA and dissociation of PA_{20}; *3*, self-association of monomeric PA_{63} to form the heptameric prepore; *4*, binding of EF/LF to the prepore; *5*, endocytosis of the receptor-PA_{63}-ligand complex; *6*, pH-dependent insertion of PA_{63} and translocation of the ligand. *B*, x-ray crystal structure of the CMG2 VWA domain, revealing a Mg^{2+} bound in the MIDAS (*gray sphere*) and a disulfide bridge (*black ball-and-stick*) linking its amino and carboxyl termini.[2] The coordinated Mg^{2+} is believed to directly interact with the acidic side chain of Asp683 in PA. *C*, CMG2 VWA domain ($CMG2^{35–225}$) purified by GST affinity chromatography, cleaved by thrombin, and further purified by size exclusion chromatography. *Lane 1*, molecular mass markers. *Lane 2*, purified $CMG2^{35–225}$ (~20 kDa).

divided the signal in channel 1 by the signal in channel 2 to obtain an apparent FRET ratio.

For association kinetics experiments, all four syringes of the stopped-flow were used. Buffer solutions contained universal buffer, which was supplemented by either 2 mM $MgCl_2$ and 2 mM EGTA, 1 mM $CaCl_2$, or 2 mM each EDTA and EGTA. All protein solutions were diluted into modified universal buffer and incubated for 1 h at room temperature. In all experiments, at least a 5-fold excess of CMG2 to PA_{83} was delivered to maintain pseudo-first order reaction conditions. Total shot volumes were 300 μl. Flow rates ranged from 7 to 15 ml s^{-1}, and the dead time was estimated at 1–2 ms. Three to four kinetic transients were averaged per rate determination.

For ultraslow dissociation kinetics experiments (10^4–10^5 s) the ISS fluorimeter was used instead of the stopped-flow. Here a 1.6-ml sample was made in universal buffer containing 50 nM PA_{83} E733C-AF488 and 100 nM $CMG2^{C40}$-AF546. At time 0, 2 μM $CMG2^{C40}$-NEM was manually added. FRET was monitored as stated above. Dissociation was reported by the loss of FRET signal due to the presence of a 20-fold excess of unlabeled $CMG2^{C40}$-NEM. Time points were taken automatically every 10 s over 3×10^4 s for Ca^{2+}-liganded complex. For Mg^{2+}-liganded complex multiple time spacing was measured over several days, first every 100 s for 5×10^4 s and then multiple time courses of 2000 s with points spaced out to 2×10^5 s.

Kinetic and Equilibrium Data Analysis—Binding association and dissociation rate constants, k_a and k_d, respectively, were obtained by fitting to a monoexponential model (Equation 1), whereas PA heptamerization kinetics were fit to a second order model (Equation 2),

$$A(t) = \mathrm{A}\exp(-k_{obs} \times t) + C \quad \text{(Eq. 1)}$$

$$A(t) = A/(1 + k_{obs} \times t) + C \quad \text{(Eq. 2)}$$

where the amplitude at time 0, A, decays with respect to time, t. The offset, C, is the final value reached when the system achieves equilibrium. For binding association kinetics, pseudo-first-order conditions are maintained, *i.e.* CMG2 concentrations are >5-fold above the concentration of PA_{83}. Observed kinetic rate constants (k_{obs}) were separately fit or averaged to obtain association and dissociation rate constants. Equilibrium dissociation constants are calculated from kinetic measurements of the association and dissociation rate constants according to $K_D = k_d/k_a$.

RESULTS

Expression and Purification of CMG2 VWA Domain—Recombinant CMG2 VWA domain ($CMG2^{35–225}$) was fused to the carboxyl terminus of GST, and the resulting GST-CMG2 fusion protein was expressed in *Escherichia coli*. The protein was affinity-purified from bacterial extract on a glutathione-Sepharose column. The protein was cleaved on the column with thrombin, releasing the CMG2 VWA domain into the fluid phase in almost pure form. After an additional size-exclusion chromatography step, the CMG2 VWA domain was obtained in high purity as judged by SDS-PAGE (Fig. 1*C*).

PA_{83} Binds 1 Stoichiometric Equivalent of CMG2 VWA Domain—We measured the stoichiometry of CMG2 VWA domain binding to PA_{83} by three independent methods, isothermal titration calorimetry, FRET-based titration, and size-exclusion chromatography coupled with multiangle laser light scattering.

For isothermal titration calorimetry measurements, PA_{83} was loaded into the measurement cell, and $CMG2^{35–225}$ was added in small increments under continuous stirring. The concentration of PA_{83} used was 5 μM, orders of magnitude above the K_d (see Table I), allowing incremental substoichiometric amounts of $CMG2^{35–225}$ to bind PA_{83} quantitatively up to the point of saturation. As shown in Fig. 2, saturation by $CMG2^{35–225}$ was achieved at approximately a one-to-one molar ratio ($1.03 \pm 5 \times 10^{-3}$).

In a second approach we used FRET to report on the binding of CMG2 VWA domain and PA_{83} under equilibrium conditions. A donor fluorophore (AF488) was attached to PA_{83} via a unique, introduced cysteine (E733C), creating PA_{83} E733C-AF488. A truncated version of CMG2, $CMG2^{R40}$, was modified on its amino terminus to have a single cysteine ($CMG2^{C40}$), which served as a unique site for fluorescent dye attachment. $CMG2^{C40}$ was labeled by the acceptor fluorophore, AF546. The donor was excited by the 488-nm Ar^+ laser line, and binding was reported by sensitized emission from the acceptor. The Förster distance, R_o, for these two fluorophores is ~60 Å; distances up to ~100 Å generate enough signal to report binding. The degree of donor quenching indicated that the donor and acceptor in the PA·$CMG2^{C40}$ complex are ~60–70 Å apart (Fig. 3*A*). The concentration of PA used (1 μM), far above the K_d, yielded a titration style plot (Fig. 3*B*). Successive additions of the acceptor CMG2 increased the FRET signal until all PA_{83} acceptor was bound, and no additional FRET was observed upon further additions. The intersection of two lines from separate linear fits to the sub-stoichiometric and saturation data defines a binding stoichiometry of 1.0 ± 0.1.

Using size-exclusion chromatography coupled with multiangle laser light scattering, the measured molecular mass of the PA_{83}·$CMG2^{35–225}$ complex, isolated as a discrete peak, was

Downloaded from www.jbc.org by on July 7, 2008

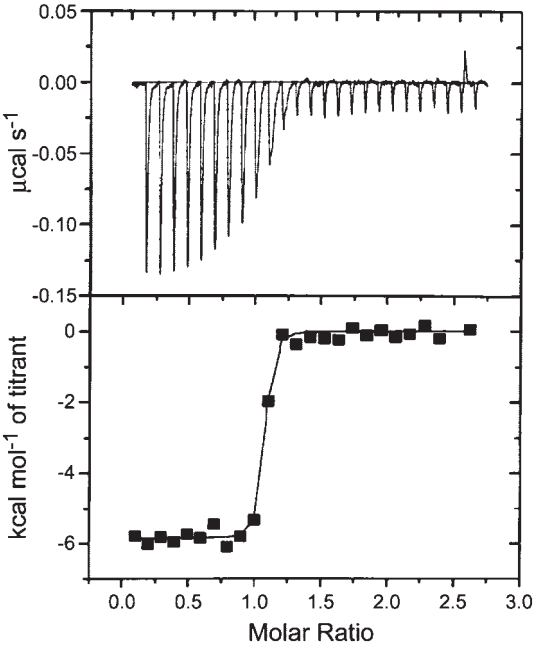

FIG. 2. **Isothermal titration calorimetry.** PA_{83} monomer (5 μM) was titrated with CMG2 (70 μM stock) at 30 °C. Molar ratio is defined as [CMG2]/[PA]. Data are fit using non-linear least squares, which determined the binding stoichiometry to be $1.03 \pm 5 \times 10^{-3}$ CMG2 per PA_{83} monomer.

98 kDa and agrees with the theoretical value, 104 kDa, for a one-to-one complex. Molecular mass values were constant across the peak, indicating homogeneity of the complex.

PA_{63} Heptamer Binds 7 Eq of $CMG2^{35–225}$—We performed a FRET binding titration assay similar to that carried out on monomeric PA_{83} to determine the number of CMG2 VWA domains that bind uniformly labeled $(PA_{63})_7$. Fluorescently labeled PA_{83} was treated with trypsin, and the PA_{63} fraction was isolated by anion-exchange chromatography. This fraction was shown earlier to be heptameric by light scattering (7) and x-ray crystallography (18). For fluorescence titrations, successive substoichiometric additions of the acceptor CMG2 increased the FRET signal until all $(PA_{63})_7$ binding sites were saturated. Subsequent additions revealed no additional FRET (Fig. 3*C*). The solution of the intersecting linear fits of data compiled from three separate titrations defines a binding stoichiometry of 7.1 ± 0.3 CMG2 VWA domains per heptamer.

Mass estimates from size-exclusion chromatography coupled with multiangle laser light scattering showed that $(PA_{63})_7$ binds at least 5 molecules of $CMG2^{35–225}$ but values of the masses were not sufficiently accurate to confirm the 7-fold stoichiometry offered by FRET. This approach suffered from the fact that the mass of each molecule of $CMG2^{35–225}$ (21 kDa) that bound to $(PA_{63})_7$ (441 kDa) is equivalent to the measurement error for this method when working in the half-million dalton range (±5%).

Does $CMG2^{35–225}$ Affect the Rate of PA_{63} Heptamerization?—We developed a second novel FRET method to monitor $(PA_{63})_7$ prepore formation in solution to test whether $CMG2^{35–225}$ affected the assembly process. In this assay donor (AF488)- and acceptor (AF546)-labeled PA_{83} were made by modifying a unique, solvent-accessible cysteine engineered at residue 563. Fluorescently labeled PA_{83} proteins were then nicked with trypsin. The heptamerization reaction mixture contained equimolar amounts of nicked donor and acceptor PA_{83} (50 nM each). At time 0, LF_N (the LF amino-terminal domain) was added (100 nM) to initiate the reaction. Control experiments verified that LF_N accelerated the heptamerization reaction.

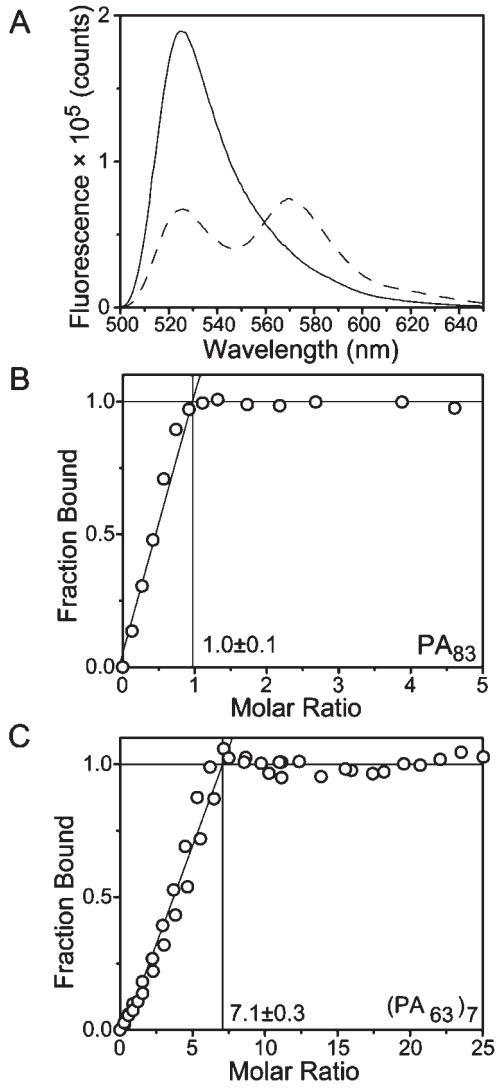

FIG. 3. **Fluorescence equilibrium stoichiometry titration assays.** *A*, FRET emission spectra (488 nm excitation) of $(PA_{63})_7$ E733C-AF488 (*solid line*) and a stoichiometric complex of $(PA_{63})_7$ E733C-AF488 and $CMG2^{C40}$-AF546 (*dashed line*). The donor emission band at ~520 is quenched upon the addition of CMG2 acceptor due to binding, and the acceptor band (~570 nm) increases in intensity, indicating resonance energy transfer. Fluorescence equilibrium binding titration of PA_{83} monomer (*B*) reveals a stoichiometry of 1.0 ± 0.1 $CMG2^{R40}$ moieties per PA_{83}, whereas heptamer (*C*) binds 7.1 ± 0.3 $CMG2^{R40}$ moieties. Molar ratio is defined as [CMG2]/[PA]. All experiments were conducted at 20 °C, and data were fit using linear least squares.

The rate of heptamerization was reported by the increase in FRET due to the incorporation of donor and acceptor PA_{63} into the $(PA_{63})_7$·LF_N complex (Fig. 4). The kinetics fit to a second order rate expression with an observed rate constant of 8.8×10^{-4} s^{-1}. We then compared the rate of heptamerization when the same equimolar mixture of nicked fluorescent PA_{83} was prebound by a 10-fold excess of $CMG2^{35–225}$. The rate constant for PA_{63} heptamerization, 7.8×10^{-4} s^{-1}, was not significantly altered by the presence of $CMG2^{35–225}$.

Binding Kinetics of CMG2 to PA_{83}—We used surface plasmon resonance (SPR) and FRET to obtain association and dissociation rate constants. For SPR studies, PA_{83} was bound to the dextran surface of a CM5 chip by amine coupling. Serial injections of $CMG2^{35–225}$ showed that it bound to the immobilized PA_{83}, and association kinetic traces were readily measured (Fig. 5*A*). Values of k_a and k_d measured with two different PA_{83} preparations and two different CM5 chips were similar.

Downloaded from www.jbc.org by on July 7, 2008

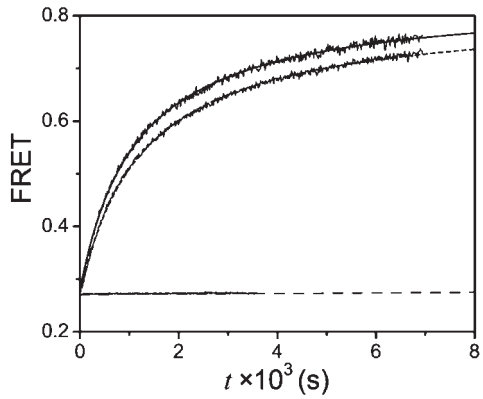

FIG. 4. **The kinetics of PA_{63} heptamerization.** For the FRET-based kinetics assay, a reaction mixture of fluorescent nicked PA_{83} (50 nM each donor, AF488, and acceptor, AF546), 1 mM Ca^{2+}, 0.1 mg/ml bovine serum albumin, pH 8.5, was preincubated with either no $CMG2^{35-225}$ (fit with a *solid line*) or 1 μM $CMG2^{35-225}$ (fit with a *short dashed line*) at 20 °C for 15 min. At time 0, each heptamerization reaction was accelerated by the addition of 100 nM LF_N. The control reaction, in the absence of LF_N (fit by *long dashed line*), shows little increase in FRET. Kinetic profiles indicate an increase in FRET due to the incorporation of donor and acceptor PA_{63} into the heptamer-LF_N complex. Profiles fit to a second order rate expression (Equation 2) with rate constants of 8.8×10^{-4} and 7.8×10^{-4} s^{-1} in the presence and absence of $CMG2^{35-225}$, respectively.

The average measured k_a for $CMG2^{35-225}$ was $1.7 \times 10^5 \pm 7 \times 10^4$ M^{-1} s^{-1}, with R^2 values greater than 0.999. The value of k_a was $7 \times 10^{-5} \pm 5 \times 10^{-5}$ s^{-1}. The slow dissociation rate made accurate measurement difficult ($R^2 = 0.41$) because the base line drifted over time, and dissociation curve measurements (up to 150 s) had to be extrapolated to 0. From the association and dissociation rate constants, we calculated the equilibrium dissociation constant, K_d, to be $4 \times 10^{-10} \pm 2 \times 10^{-10}$ M.

Additional SPR measurements were made on $CMG2^{R40}$, a truncated construct, lacking the natural disulfide bond between Cys-39 and Cys-218. This association rate, measured in the presence of Ca^{2+}, was found to be about 2-fold slower than $CMG2^{35-225}$ (Fig. 5*C*). Reduction of the disulfide bond in $CMG2^{S38}$ similarly reduced the association rate by a factor of 2 with respect to the oxidized form (Table I).

Because of the inherent difficulties in measuring extremely slow dissociation rates (lifetimes >, 10^4 s) using SPR, we developed a FRET-based binding system. Association rates were initially estimated using stopped-flow to confirm the fidelity of the novel VWA domain binding assay. Blue laser light was used to excite the donor fluorophore (AF488) on PA, which transferred energy to the acceptor fluorophore (AF546) on $CMG2^{C40}$, allowing binding kinetics to be observed (Fig. 5*B*). Association rate constants (k_a) measured for this FRET-based system ($1.1 \times 10^5 \pm 5 \times 10^3$ M^{-1} s^{-1}) were similar to those measured by SPR using $CMG2^{R40}$ in the presence of Ca^{2+} (Fig. 5*C*).

The dissociation rate was monitored using non-fluorescent $CMG2^{C40}$-NEM (where the reactive cysteine was blocked by *N*-ethylmaleimide). Here, PA_{83} E733C-AF488 and $CMG2^{C40}$-AF546 were preincubated with 1 mM Ca^{2+} buffer, and equivalent amounts were mixed to form a complex. The exchange reaction was initiated by adding a 20-fold excess of $CMG2^{C40}$-NEM competitor. Kinetics, monitored over the course of 3×10^4 s, fit to a dissociation rate constant of $8.4 \times 10^{-5} \pm 5 \times 10^{-7}$ s^{-1} (Fig. 5*D*). Thus, the K_d is $7.8 \times 10^{-10} \pm 3 \times 10^{-11}$ M.

Taking advantage of this FRET system, we also measured the association rates of Mg^{2+}-bound CMG2. Here, protein solutions were preincubated with 2 mM $MgCl_2$ and 1 mM EGTA, reducing the effective concentration of even 1 μM contaminating Ca^{2+} to less than 1 pM. Surprisingly, the association rate constant in the presence of Mg^{2+}, as compared with Ca^{2+}, is 2 times slower, at $5.3 \times 10^4 \pm 9 \times 10^2$ $M^{-1}s^{-1}$. Nonetheless, the dissociation rate was 10-fold slower ($9.2 \times 10^{-6} \pm 1 \times 10^{-7}$ s^{-1}; Fig. 5*D*), yielding a K_d of $1.7 \times 10^{-10} \pm 9 \times 10^{-13}$ M.

Finally, we conducted binding kinetics experiments in metal ion "free" buffer that contains 2 mM EDTA and EGTA to chelate and sequester metal ions bound in the MIDAS motif and those contaminating the buffer solutions. The observed rate constants (k_{obs}), plotted in Fig. 5*C*, demonstrate a "non-linear" CMG2 concentration dependence (in the log-log plot), indicating that the [CMG2] used in the measurements is on the order of the K_d. The observed rate constant, k_{obs}, for binding is the sum of the association and dissociation rates,

$$k_{obs} = k_d + k_a \times [L] \quad \text{(Eq. 3)}$$

where only the association rate is dependent on the concentration of free ligand, [L]. The observed rates may then be fit by Equation 3 to obtain both the association and dissociation rate constants, $9.3 \times 10^4 \pm 7 \times 10^3$ M^{-1} s^{-1} and $8.6 \times 10^{-2} \pm 4 \times 10^{-3}$ s^{-1}, respectively. This model fit well, with an R^2 value of 0.85, and generates a K_d of $9.6 \times 10^{-7} \pm 8 \times 10^{-8}$ M.

Thermodynamic Contribution of the Metal Ion Site—Because the affinity of CMG2 for PA could be measured in both the presence and absence of metal ions, the energetic contribution of the metal ion could be determined. This measurement is unique to our study of VWA domain binding, because often the removal of metal ions from the MIDAS completely abrogates binding. Knowing the affinity in the absence of metal ions allows the calculation to be made according to Equation 4,

$$\Delta\Delta G^{M2+} = RT\ln(K_d^{M2+}/K_d) \quad \text{(Eq. 4)}$$

in which the equilibrium dissociation constant in the absence (K_d) and presence of a metal ion (K_d^{M2+}) are known. R and T are the gas constant and temperature, respectively. This model also assumes that the MIDAS is saturated, and the metal ion cannot freely exchange with the buffer, because it is buried in the binding interface. Estimates of $\Delta\Delta G^{M2+}$ due to the presence of the bridging metal ion found in the MIDAS of CMG2 are -5.1 ± 0.05 and -4.2 ± 0.05 kcal mol^{-1} for Mg^{2+} and Ca^{2+}, respectively.

DISCUSSION

In the current study we have prepared soluble CMG2 VWA domain and quantitatively examined its interaction with monomeric and heptameric forms of PA. We studied the binding kinetics, the thermodynamics, and the role of metal ion in the interaction.

Binding Stoichiometry to Monomeric and Oligomeric Forms of PA—We quantified the number of $CMG2^{35-225}$ molecules bound to various forms of PA using three independent methods. All revealed that one $CMG2^{35-225}$ binds per PA_{83} monomer. CMG2 binding stoichiometry for PA heptamer was measured using a FRET method identical to that used on PA_{83} monomer. Titrations of labeled $CMG2^{C40}$ at concentrations 100-fold greater than the K_d demonstrate that seven $CMG2^{C40}$ moieties bind per heptamer. These results indicate that the heptamerized form of PA_{63} does not preclude simultaneous occupancy of its seven individual CMG2 VWA domain binding sites, for example by steric obstruction.

Correspondingly, FRET studies on the heptamerization of PA_{63} (Fig. 4) reveal that the rate of complex assembly in solution is not significantly different when PA monomer is liganded by $CMG2^{35-225}$. This result supports the FRET binding stoichiometry studies on heptamer; if the heptameric form of PA could bind less than seven CMG2 VWA domains due to steric constraints, then the rate of assembly, $\sim 10^{-3}$ s^{-1}, would be reduced, because CMG2 VWA domains would have to dissociate

Downloaded from www.jbc.org by on July 7, 2008

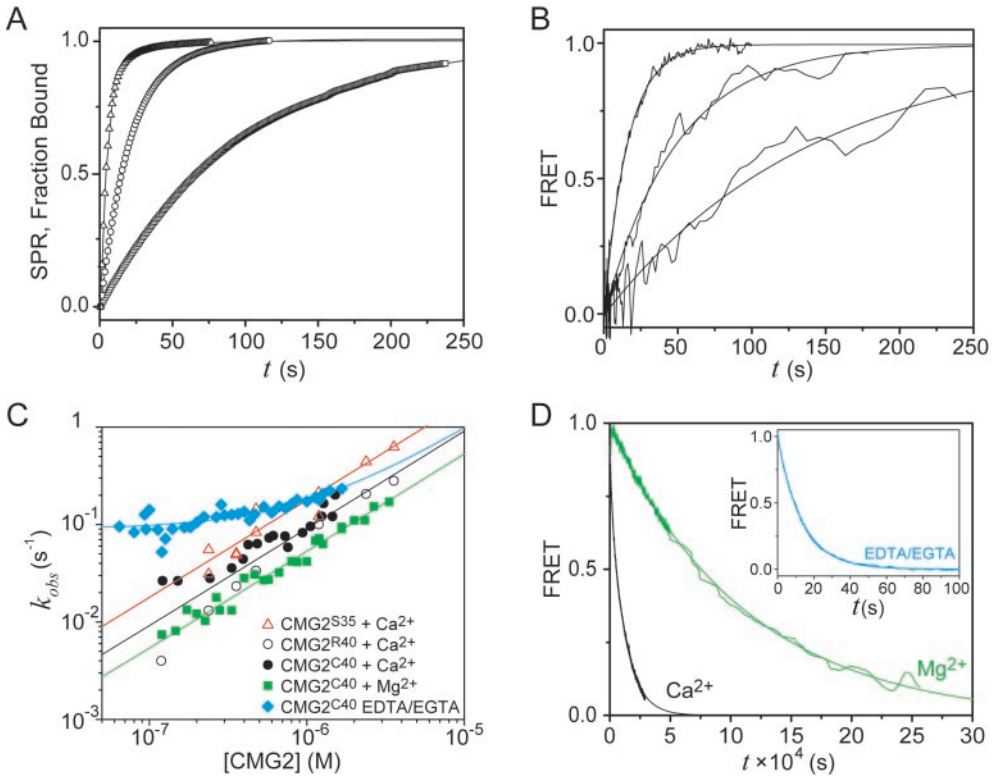

FIG. 5. **SPR, stopped-flow FRET, and ultra-slow FRET kinetics measurements.** *A*, SPR was used to monitor rates of association of Ca^{2+}-liganded $CMG2^{35–225}$ to surface-bound PA_{83}. Representative traces fit to exponential decays at 1.19 μM, 357 nM, and 119 nM (from fastest to slowest). *B*, stopped-flow FRET was used to monitor rates of association of Ca^{2+}-liganded $CMG2^{C40}$-AF546 to PA_{83} E733C-AF488. Representative traces fit to exponential decays at 490, 100, and 36 nM (from fastest to slowest). *C*, observed rate constants, k_{obs}, from binding kinetics experiments as a function of CMG2 concentration for SPR and stopped-flow FRET. SPR k_{obs} for $CMG2^{35–225}$ in Ca^{2+} (*red open triangle*) and $CMG2^{R40}$ in Ca^{2+} (*black open circle*) are shown. Stopped-flow FRET k_{obs} for $CMG2^{C40}$ in Ca^{2+} (*black filled circle*), Mg^{2+} (*green filled square*), and a metal ion-free condition of 2 mM each EDTA and EGTA (*blue filled diamond*) are shown. Parameters of curve fits using Equation 3 are in Table I; only association rate constants are fit for Ca^{2+}- and Mg^{2+}-liganded complexes since the dissociation rate constant is a fixed parameter from that observed in separate dissociation experiments (see *D*); both the association and dissociation rate constants are fit for the EGTA/EDTA, metal ion-free complex. *D*, FRET-based dissociation kinetics experiments in which fluorescently labeled complex (50 nM) is competed with 2 μM $CMG2^{R40}$-NEM, where complex was either preassembled in Ca^{2+} (*black line*) or Mg^{2+} (*green line*). *Inset*, FRET-based dissociation kinetics experiment (*blue line*) in which 200 nM fluorescently labeled complex (200 nM labeled PA with 2 μM labeled $CMG2^{C40}$) preassembled in 2 mM each EDTA and EGTA is diluted ~10-fold into buffer containing ~2 μM $CMG2^{R40}$-NEM using stopped-flow. All dissociation kinetics data are fit to monoexponentials. All metal ion solution concentrations are effectively 1 mM, and all kinetics experiments were carried out at 20 °C.

TABLE I
Kinetic and thermodynamic parameters for binding of CMG2 to PA_{83}

Protein	Metal ion buffer	Method	k_a	k_d	K_d	$\Delta\Delta G^{M2+}$
			$M^{-1}\ s^{-1}$	s^{-1}	M[a]	*kcal mol*$^{-1}$
$CMG2^{35–225}$	1 mM Ca^{2+}	SPR	$1.7 \times 10^5 \pm 7 \times 10^4$	$7 \times 10^{-5} \pm 5 \times 10^{-5}$	$4 \times 10^{-10} \pm 2 \times 10^{-10}$	ND[b]
$CMG2^{S38}$ Reduced S-S[c]	1 mM Ca^{2+}	SPR	$9.0 \times 10^4 \pm 7 \times 10^3$	ND	ND	ND
$CMG2^{R40}$	1 mM Ca^{2+}	SPR	$8.1 \times 10^4 \pm 2 \times 10^3$	$4 \times 10^{-5} \pm 2 \times 10^{-5}$	$5 \times 10^{-10} \pm 2 \times 10^{-10}$	ND
$CMG2^{C40}$-AF546	1 mM Ca^{2+}	FRET	$1.1 \times 10^5 \pm 5 \times 10^3$	$8.4 \times 10^{-5} \pm 5 \times 10^{-7}$	$7.8 \times 10^{-10} \pm 3 \times 10^{-11}$	-4.2 ± 0.05
$CMG2^{C40}$-AF546 1 mM EGTA	2 mM Mg^{2+}	FRET	$5.3 \times 10^4 \pm 9 \times 10^2$	$9.2 \times 10^{-6} \pm 1 \times 10^{-7}$	$1.7 \times 10^{-10} \pm 9 \times 10^{-13}$	-5.1 ± 0.05
$CMG2^{C40}$-AF546 2 mM EGTA	2 mM EDTA	FRET	$9.3 \times 10^4 \pm 7 \times 10^3$	$8.6 \times 10^{-2} \pm 4 \times 10^{-3}$	$9.6 \times 10^{-7} \pm 8 \times 10^{-8}$	ND

[a] The equilibrium dissociation constant is calculated from kinetic measurements of the association and dissociation rate constants according to $K_d = k_d/k_a$.
[b] ND, not determined.
[c] Natural disulfide (Cys-39–Cys-218) is reduced by 0.5 mM tris-(2-carboxyethyl)phosphine.

at the slower rate, $\sim 10^{-5}\ s^{-1}$, before assembly. In solution, the assembly of PA heptamer is not directly facilitated by the presence of CMG2 VWA domain. The modest 11% reduction in rate may reflect some minor steric or electrostatic repulsion from CMG2 VWA domain moieties in the assembly process.

Binding Affinity of CMG2 to PA—SPR measurements with $CMG2^{35–225}$ yielded K_d values ~400 pM in the presence of Ca^{2+}. Stopped-flow FRET measurements on a truncated, disulfide-free version ($CMG2^{C40}$) gave a K_d of 780 pM in the presence of Ca^{2+}; however, when studied in the presence of a 1 mM effective concentration of Mg^{2+}, the K_d became significantly tighter, 170 pM (Table I).

Our observation that the CMG2-PA binding interaction prefers Mg^{2+} to Ca^{2+} by 5-fold differs from a previous study (11). The enzyme-linked immunosorbent assay-based assay used in that study may have more closely sensed the 2-fold slower association rate for Mg^{2+} with respect to Ca^{2+} that we observed, thereby underestimating the affinity as Mg^{2+}-bound

Downloaded from www.jbc.org by on July 7, 2008

complex dissociates 10-fold more slowly. Alternatively, the discrepancy may reflect differences in the constructs used in the two studies; the construct used in the enzyme-linked immunosorbent assay had 15 additional residues on the carboxyl terminus. Recent x-ray crystallographic studies of CMG2 reveal a coordinated Mg^{2+} in the MIDAS (Fig. 1*B*).[2] Other crystallographic studies show that many different divalent metal ions may be exchanged into a VWA domain MIDAS (19), although the Ser and Thr side chains of the MIDAS generally disfavor direct Ca^{2+} coordination (20).

Thermodynamic Implications of CMG2 MIDAS—By comparing K_d values in the presence and absence of metal ions, we determined that the Mg^{2+}-bound form of CMG2 stabilizes the complex of PA and CMG2 by ~5 kcal mol^{-1}. This large increase in binding affinity argues strongly that the MIDAS motif directly coordinates PA via the metal ion. The coordination of the MIDAS metal often involves a glutamic or aspartic acid residue from the ligand (20). Consistent with this model, several studies indicate that mutations at Asp-683 in domain 4, the receptor binding domain of PA, compromise receptor binding (21–23), implicating this residue for that role. Also, if CMG2 MIDAS metal ion is geometrically modeled to bind PA via Asp-683, then the predicted distance between Glu-733 on PA and the amino terminus of CMG2 is ~60 Å, consistent with the distance calculated from the observed FRET efficiency (Fig. 3*A*).

Binding Studies on Other VWA Domains—Multiple ligand binding equilibrium and kinetics studies have been reported for the interactions of VWA domains for their endogenous, physiological ligands. Association rates vary from 1 to 10^5 M^{-1} s^{-1}, dissociation rates vary from 10 s^{-1} to 10^{-2} s^{-1}, and K_d values range from millimolar to submicromolar (20, 24–27). Affinity of CMG2, 170 pM, however, is 1000-fold greater in stability than the tightest of these reported physiological VWA domain-ligand interactions.

The VWA domains from α-integrins can augment their binding affinity via a conformational switch. This switch from an open (high affinity) to a closed (low affinity) conformation in α-integrin VWA domains is thought to be important to their cellular function (20, 24, 26, 27). The closed form involves an acidic side chain from the VWA domain that directly coordinates the metal ion and competitively blocks access of the ligand. Such a mechanism would tend to reduce the association rate of the binding reaction according to the scheme, in Equations 5 and 6.

$$\text{Closed} \leftrightarrow \text{Open} \qquad \text{(Eq. 5)}$$

$$\text{Open} + \text{ligand} \leftrightarrow \text{Complex} \qquad \text{(Eq. 6)}$$

The tight binding and rapid association rate (10^5 $M^{-1}s^{-1}$) for CMG2 VWA domain with PA suggest that CMG2 thermodynamically prefers to be in the open, high affinity state. Recent x-ray crystallographic studies on the CMG2 VWA domain reveal two structures that align well with the open, high affinity forms of α-integrin.[2] Proteins stabilized by specific engineered disulfides into the open conformation show association rates that plateau at about 2×10^5 M^{-1} s^{-1}, similar to that observed for $CMG2^{35–225}$ (Fig. 5*C*; Table I). The kinetic and structural observations suggest that the CMG2 VWA domain, when liganded by divalent metal ion, either energetically favors the open, high affinity state or structurally is unable to occupy the closed form.

The natural disulfide in the CMG2 VWA domain (Fig. 1*B*), however, does not significantly stabilize the open conformation. Either breaking the natural disulfide bond in $CMG2^{S38}$ with strong reductant or using a truncated version lacking the disulfide showed only a 2-fold reduction in association rate (Table I). The K_d of versions lacking the disulfide did not significantly decrease, and therefore, other features of the CMG2 VWA domain structure must explain why it more heavily populates the open conformation.

Why Is the Affinity So Tight?—CMG2 VWA domain rapid association rate is consistent with an open configuration (Equations 5 and 6), yet the K_d is 1000-fold greater than the binding affinities of VWA domains (submicromolar K_d values), which were optimized by engineered disulfides. Therefore, the increased affinity in the PA·CMG2 interaction is not fully explained by CMG2 thermodynamic preference for the open conformation, but, rather, the increase arises from its uncharacteristically slow dissociation rate. Furthermore, the observation of significant residual submicromolar affinity in the absence of metal ions supports the argument that the ligand, PA, contributes additional binding surface beyond the typical VWA domain-ligand interface. Secondary determinants, outside of the MIDAS motif, may have evolved in PA to augment the stability of the interaction. Two possible structural models become apparent. (i) The burial of additional surface in and around the metal ion binding site, for example, may prevent water molecules from accessing and competing for the coordinating metal ion. (ii) Alternatively, or in conjunction with the previous model, additional hydrophobic surface burial or electrostatic contacts more distant from the MIDAS motif may provide a second source of increased binding energy.

Other Tight Binding VWA Domain Host-Pathogen Interactions—The slow rate of dissociation observed for the CMG2·PA complex is uncharacteristic of many VWA domain complexes with their physiological ligands, but it is not unique for a host-pathogen interaction. The neutrophil inhibitory factor (NIF) of hookworm, *Ancylostoma canium,* which is a potent inhibitor of adhesion-dependent function in neutrophils (*e.g.* phagocytosis, chemotaxis, and spreading), binds to the VWA domain of the integrin CR3 (CD11b) with ~1 nM affinity due to a slow dissociation rate, 10^{-5} s^{-1} (28, 29). The divalent metal ion dependence for NIF·CD11b was less significant, *i.e.* ~2–5-fold reduced in the absence of metal ions (28, 29), whereas we observed a 6000-fold reduction in affinity for PA·CMG2. NIF and PA may bind their receptor VWA domain in a metal ion-independent manner but to very different degrees, consistent with the model that a second MIDAS-independent binding surface is utilized by CMG2. The tight binding strategy adopted by NIF clearly aims to block and inhibit adhesion-dependent responses of the neutrophil by competitively binding host integrin VWA domains (28).

The CMG2 Role in Toxin Assembly and Translocation—The high affinity and extremely slow dissociation rate of the PA·CMG2 VWA domain interaction, on the other hand, facilitates toxin assembly and translocation (Fig. 1*A*). For monomeric PA, the average lifetime of the dissociation, $1/k_a$, for Mg^{2+}-liganded CMG2 VWA domain is ~30 h. Thermodynamically, when considering the 7-fold stoichiometry of CMG2-liganded heptamer, the additive metal ion binding free energy $\Delta\Delta G^{M2+}$ for seven independent PA·CMG2 interactions is 35 kcal mol^{-1}, favoring bound prepore heptamer to free by a factor of 10^{25}.

During anthrax intoxication, PA must remain bound initially to the extracellular membrane surface and subsequently to the inner surface of a vesicle during the translocation process. An initial role of the receptor may be to increase the cell surface concentration of PA monomer, thereby promoting heptamer formation. Second, the receptor ensures that heptamer remains bound to the cell, allowing EF and LF to bind and assemble into a complex. Finally, tight affinity presumably permits anthrax toxin to assemble and translocate active LF

Downloaded from www.jbc.org by on July 7, 2008

and EF proteins in the very earliest stages of the intoxication, even when these proteins are low in concentration.

The CMG2 ~200 pM affinity for PA may also be exploited therapeutically as a potent anti-toxin. The tight binding and slow dissociation kinetics indicate that the CMG2 VWA domain may be delivered in soluble form to compete for the domain 4 binding site on monomeric PA_{83}, blocking the PA ability to bind receptors, assemble, and translocate the enzymatic effectors, LF and EF, into target cells.

Acknowledgments—We thank L. Greene and R. Pimental for assistance in purifying proteins, J. A. T. Young, H. Scobie, and J. Rainey for the CMG2 clone and critical comments on the manuscript, and T. Sosnick for his critical reading of the manuscript.

REFERENCES

1. Duesbery, N. S., Webb, C. P., Leppla, S. H., Gordon, V. M., Klimpel, K. R., Copeland, T. D., Ahn, N. G., Oskarsson, M. K., Fukasawa, K., Paull, K. D., and Vande Woude, G. F. (1998) *Science* **280,** 734–737
2. Vitale, G., Pellizzari, R., Recchi, C., Napolitani, G., Mock, M., and Montecucco, C. (1998) *Biochem. Biophys. Res. Commun.* **248,** 706–711
3. Leppla, S. H. (1982) *Proc. Natl. Acad. Sci. U. S. A.* **79,** 3162–3166
4. Molloy, S. S., Bresnahan, P. A., Leppla, S. H., Klimpel, K. R., and Thomas, G. (1992) *J. Biol. Chem.* **267,** 16396–16402
5. Milne, J. C., Furlong, D., Hanna, P. C., Wall, J. S., and Collier, R. J. (1994) *J. Biol. Chem.* **269,** 20607–20612
6. Elliott, J. L., Mogridge, J., and Collier, R. J. (2000) *Biochemistry* **39,** 6706–6713
7. Mogridge, J., Cunningham, K., and Collier, R. J. (2002) *Biochemistry* **41,** 1079–1082
8. Friedlander, A. M. (1986) *J. Biol. Chem.* **261,** 7123–7126
9. Abrami, L., Liu, S., Cosson, P., Leppla, S. H., and van der Goot, F. G. (2003) *J. Cell Biol.* **160,** 321–328
10. Blaustein, R. O., Koehler, T. M., Collier, R. J., and Finkelstein, A. (1989) *Proc. Natl. Acad. Sci. U. S. A.* **86,** 2209–2213
11. Scobie, H. M., Rainey, G. J. A., Bradley, K. A., and Young, J. A. (2003) *Proc. Natl. Acad. Sci. U. S. A.* **100,** 5170–5174
12. Bradley, K. A., Mogridge, J., Mourez, M., Collier, R. J., and Young, J. A. (2001) *Nature* **414,** 225–229
13. Whittaker, C. A., and Hynes, R. O. (2002) *Mol. Biol. Cell* **13,** 3369–3387
14. Lee, J. O., Rieu, P., Arnaout, M. A., and Liddington, R. (1995) *Cell* **80,** 631–638
15. Croney, J. C., Cunningham, K. M., Collier, R. J., and Jameson, D. M. (2003) *FEBS Lett.* **550,** 175–178
16. Barnard, A., and Payton, M. (1995) in *Current Protocols in Protein Science* (Coligan, J. E., Dunn, B. M., Plough, H. L., Speicher, D. W., and Wingfield, P. T., eds) Vol. 5.3, pp. 1–18, John Wiley & Sons, Inc.
17. Cunningham, K., Lacy, D. B., Mogridge, J., and Collier, R. J. (2002) *Proc. Natl. Acad. Sci. U. S. A.* **99,** 7049–7053
18. Petosa, C., Collier, R. J., Klimpel, K. R., Leppla, S. H., and Liddington, R. C. (1997) *Nature* **385,** 833–838
19. Liddington, R., and Bankston, L. (1998) *Structure* **6,** 937–938
20. Shimaoka, M., Takagi, J., and Springer, T. A. (2002) *Annu. Rev. Biophys. Biomol. Struct.* **31,** 485–516
21. Mourez, M., Yan, M., Lacy, D. B., Dillon, L., Bentsen, L., Marpoe, A., Maurin, C., Hotze, E., Wigelsworth, D., Pimental, R. A., Ballard, J. D., Collier, R. J., and Tweten, R. K. (2003) *Proc. Natl. Acad. Sci. U. S. A.* **100,** 13803–13808
22. Bradley, K. A., Mogridge, J., Rainey, G. J. A., Batty, S., and Young, J. A. (2003) *J. Biol. Chem.* **278,** 49342–49347
23. Rosovitz, M. J., Schuck, P., Varughese, M., Chopra, A. P., Mehra, V., Singh, Y., McGinnis, L. M., and Leppla, S. H. (2003) *J. Biol. Chem.* **278,** 30936–30944
24. McCleverty, C. J., and Liddington, R. C. (2003) *Biochem. J.* **372,** 121–127
25. Lupher, M. L., Jr., Harris, E. A., Beals, C. R., Sui, L. M., Liddington, R. C., and Staunton, D. E. (2001) *J. Immunol.* **167,** 1431–1439
26. Shimaoka, M., Lu, C., Palframan, R. T., von Andrian, U. H., McCormack, A., Takagi, J., and Springer, T. A. (2001) *Proc. Natl. Acad. Sci. U. S. A.* **98,** 6009–6014
27. Shimaoka, M., Xiao, T., Liu, J. H., Yang, Y., Dong, Y., Jun, C. D., McCormack, A., Zhang, R., Joachimiak, A., Takagi, J., Wang, J. H., and Springer, T. A. (2003) *Cell* **112,** 99–111
28. Rieu, P., Ueda, T., Haruta, I., Sharma, C. P., and Arnaout, M. A. (1994) *J. Cell Biol.* **127,** 2081–2091
29. Muchowski, P. J., Zhang, L., Chang, E. R., Soule, H. R., Plow, E. F., and Moyle, M. (1994) *J. Biol. Chem.* **269,** 26419–26423

Downloaded from www.jbc.org by on July 7, 2008